A new methodology inspired from the Theory of Critical Distances for determination of inherent tensile strength and fracture toughness of rock materials

S. Aligholi, Laurent Ponson, Q.B. Zhang, A.R. Torabi

A new methodology inspired from the theory of critical distances for determination of inherent tensile strength and fracture toughness of rock materials

S. Aligholi [a,*], L. Ponson [b], A.R. Torabi [c], Q.B. Zhang [a]

[a] *Department of Civil Engineering, Monash University, VIC 3800, Australia*

[b] *Fracture Lab, Institut Jean le Rond d'Alembert, CNRS – Sorbonne Université, Paris, France*

[c] *Fracture Research Laboratory, Faculty of New Science and Technologies, University of Tehran, Tehran, Iran*

Abstract

Measuring the intrinsic fracture properties of quasi-brittle materials like rocks is of great importance and at the same time a major issue for engineers. In this study, we explore the ability of the Theory of Critical Distances (TCD) to determine accurately both the tensile strength and the fracture toughness. To this end, we conduct ring tests and semi-circular bend tests on four rock types including a red sandstone, a white coarse-grained marble, a fine-grained granite and a coarse-grained granite. This selection covers sedimentary, metamorphic and igneous rock types with different grain sizes. The experimental data are analysed using a new methodology developed from the so-called Point Method (PM), a particular form of the TCD, from which we infer the intrinsic tensile strength and the fracture toughness of the studied rock materials. Our results are compared with those obtained from the methodology recommended by ISRM that is modified to take into account the finite notch root radius used in our experiments. The comparison is successful, supporting that the newly developed methodology is suitable to determine the intrinsic tensile strength and the fracture toughness of rock materials.

Keywords: Critical distance, Intrinsic tensile strength, Fracture toughness, Point method, Notch mechanics

[*] Corresponding Author:
E-mail address: aligholisaeed1@gmail.com ; saeed.aligholi@monash.edu

1. Introduction

Rocks are archetypes of quasi-brittle materials. Under compression, they generally show a rather extended non-linear regime owing to the spreading of micro-fractures before final failure takes place. Under traction, they fail through the propagation of a crack that grows through the coalescence of micro-cracks localized at the crack tip vicinity in the so-called process zone. If the spatial extent of the process zone is small with respect to the specimen size, this phenomenon is then appropriately described by the theory of Linear Elastic Fracture Mechanics (LEFM).[1] Within the LEFM framework, we introduce the fracture toughness K_{Ic} that quantifies the ability of the material to resist to crack growth. Alternatively, one can seek to determine the stress level at which the material fails in traction, thus defining the material tensile strength. This is of particular relevance in absence of an initial crack in the structure.[2,3] However, defining an intrinsic (specimen independent) tensile strength for quasi-brittle solids is a rather difficult challenge, as the load-bearing capacity of quasi-brittle specimens is known to strongly depend on its size,[4,5] and often overlooked in engineering practice.[6]

Owing to their quasi-brittle nature, rock made structures can give rise to catastrophic failures. Therefore, the accurate determination of their failure properties is key to assess the structural resistance of rock masses, an important issue in many rock engineering practices such as tunnelling, rock cutting processes, hydraulic fracturing and rock slope stability.[7] In the following, the term *structural* properties is used when the geometrical features of the specimens or bodies do play a significant role on top of the *intrinsic* properties that depend only on the microstructural features of the rock materials as well as the surrounding environment.[8]

A suitable solution for defining the tensile strength of rocks consists in considering the characteristic stress level at which the material fails within the process zone of a stress concentrator or a running crack. According to the Cohesive Zone Model (CZM) for brittle cracks,[9-10] the so-called cohesive strength σ_{c} of the material is then related to the material fracture toughness via the cohesive length ℓ_{c} (or process zone size along the crack propagation direction) through the relation $K_{\mathrm{Ic}} \propto \sigma_{\mathrm{c}}\sqrt{\ell_{\mathrm{c}}}$.[9] Although appealing, this definition raises serious experimental issues: how to determine the stress level at the tip of stress concentrators, as the process zone is hardly larger than 1 mm in most quasi-brittle specimens.

Theoretically speaking, specimens without stress concentrator could be tested under direct tension to determine the material tensile strength while specimens with sharp cracks can be used to measure the material fracture toughness. However, in practice, such a procedure is neither reliably achievable nor practical. On the one hand, it turns out that specimens without stress concentrators cannot be used to determine the tensile strength of rock materials. The reasons behind this observation have been largely discussed by researchers [e.g. 4, 11] and relates to the stochastic (defect driven) nature of tensile failure. On the other hand, preparing sharp cracks in rock specimens is a challenging task.

Considering these issues, new methodologies based on different concepts have been proposed to reliably determine the tensile strength and fracture toughness of different materials including rocks. One of them is the so-called Theory of Critical Distances (TCD) based on notch mechanics. It aims at providing simple and practical tools to engineers including rock engineers. TCD includes a group of theories used for predicting the effects of stress concentrators on material behaviour under mechanical loads.[12] The TCD can take different forms and has been used with success in a wide range of engineering problems to determine or predict properties of different materials including composites,[13-14] metals,[15-17] polymers,[18-19] and rocks.[20-23] The TCD can circumvent the experimental difficulties encountered when it comes to determining the intrinsic tensile strength and fracture toughness of quasi-brittle materials. With such an approach, specimens without stress concentrators or perfectly sharp cracks are not required to determine these properties, as we will show in the following. Furthermore, notch mechanics can be applied to modify the effect of a round-tip notch on apparent fracture toughness of materials and provide engineers with accurate values of fracture toughness,[24-27] as also detailed later.

This paper is organized as follows. First, we present the studied rock materials as well as the experimental and analytical methods adopted for this study. A brief theoretical background on the methodology employed to analyse the ring tests and bending tests carried in this study is provided in Section 2. Section 3 presents our main results including a discussion. Finally, the conclusions of our study are drawn in Section 4.

2. Materials and Methods

Four different rock types including a red sandstone, a white coarse-grained marble, a fine-grained granite and a coarse-grained granite are selected for this study. This selection covers sedimentary, metamorphic and igneous rock types with different grain sizes. The PM form of the TCD is applied to measure accurately the failure properties of these rock materials including tensile strength and fracture toughness. To check the validity of the proposed PM, the fracture toughness of the tested rocks is also measured according to the ISRM Suggested Method [28] modified to take into account the finite radius of the notch used in our experiments.

2.1. A modified version of the PM based on CZM

The PM is the simplest form of the TCD.[29] Its failure criterion has been defined by Taylor [30] as follows: 'Failure will occur when the stress at a distance $L/2$ from the notch root is equal to σ_0'. This translates as:

$$\sigma(L/2) = \sigma_0 \quad (1)$$

where L is a characteristic distance, and σ_0 is the inherent tensile strength of the material. If the stress distribution ahead of a stress concentrator and the characteristic distance are known, then the inherent tensile strength can be determined. As justified in Appendix A, the material fracture toughness K_{Ic} can finally be estimated from the relation:

$$L = \frac{1}{\pi}\left(\frac{K_{\mathrm{Ic}}}{\sigma_0}\right)^2 \tag{2}$$

Although the PM has been successfully applied to a large range of fracture problems, it remains a phenomenological method.[30] Interestingly, it is intimately connected to the CZM of failure, which rigorously extends LEFM to elasto-damageable solids. In its simplest version, CZM introduces a cohesive stress σ_{c}, below which the material behaves elastically and beyond which it does not sustain any mechanical load. This approach predicts the spatial extent of the fracture process zone, also called the cohesive zone, through the Dugdale–Barenblatt (D–B) formula (see Appendix A):[9,31]

$$\ell_{\mathrm{c}} = \frac{\pi}{8}\left(\frac{K_{\mathrm{Ic}}}{\sigma_{\mathrm{c}}}\right)^2 \tag{3}$$

This formula is almost identical to Eq. (2) up to a constant $\pi^2/8 \approx 1.23$. On top of it, considering the tensile stress distribution $\sigma(r) = K_{\mathrm{I}}/\sqrt{2\pi r}$ ahead of a running crack as predicted by LEFM, one infers the relation $\sigma(4\ell_{\mathrm{c}}/\pi^2) = \sigma_{\mathrm{c}}$ that is similar to Eq. (1). In the following, we use Eq. (3) instead of Eq. (2), as it derives from a well-identified assumption, namely the existence of a unique stress level that provides both the elastic limit and the failure threshold of the material, but we use the following PM based methodology to determine both σ_{c} and ℓ_{c}.

Specimens with different notch geometries are loaded up to failure. Following Eq. (1), the point of intersection of the stress distribution ahead of the stress concentrators at the onset of failure is expected to provide the material tensile strength. Following the previous interpretation of the PM based on CZM, two extreme stress concentrators, i.e. a sharp notch (very high-stress concentration) and a flat free surface (no stress concentration), are best suited. However, in practice, machining very sharp notches and initiating a crack from a flat free surface are quite difficult to achieve in rock materials.

To circumvent these difficulties, Semi-Circular Bend (SCB) specimens with a notch root radius of about 350μm and ring specimens with an inner radius of around 14mm are used to produce the highest and lowest possible stress concentrations, respectively. Despite the discrepancy between these specimens and the perfect

concentrators expected theoretically, our method provides accurate values of tensile strength, as we will show in Section 3.

2.2. Ring test

Rock rings are used in the following as the low-stress concentrator specimens. This test geometry has been used in the past to measure the apparent tensile strength of rocks and other brittle materials.[32,33] Note however the apparent tensile strength is a structure-dependent property rather than an inherent material property.[11, 34] The difference between the value of the apparent tensile strength and σ_c results from the combination of three factors: (1) the probabilistic nature of the resistance of materials to tensile loading; (2) the complexity of the failure process involving the initiation of a crack by damage accumulation before it can propagate; and (3) the calculated stress following a linear elastic assumption may not be the 'real' stress experienced by the material.[11]

The minimum diameter of the internal hole that could be drilled into the sandstone and the marble is about 3mm, while it is about 6mm for granites (Fig. 1-c). Rings with four different inner diameters are prepared for the sandstone and the marble, whereas three different ring specimens are prepared for granites. Moreover, normal disk specimens with no hole are also prepared and tested for all rock types. At least three different specimens for any geometry are tested and the average of calculated tensile strengths for each rock type/geometry is used for further analyses. The outer diameter and thickness of the rings/disks are around 75 and 30 mm, respectively. Note that, following the analysis of Fillon,[35] the ratio of the inner to the outer diameter of our ring specimens is less than or equal to 0.4 so that the tensile mode of failure dominates over the compressive one.[32] The driving rate of the cross-head for all our tests is set to 0.05 mm/min.

The apparent tensile strength $\sigma_{\max}$ is defined as the maximum stress level applied locally to the material at the onset of failure, assuming that it behaves elastically everywhere. It then follows:

$$\sigma_{\max} = \frac{P_{\max}}{\pi B R_0}[6 + 38(R/R_0)^2] \tag{4}$$

that provides the tensile stress applied to the inner surface of the specimen at the applied failure load $P_{\max}$. For disk specimens for which $R = 0$, the maximum applied stress is located at the center of the specimen and follows:

$$\sigma_{\max} = \frac{P_{\max}}{\pi B R_0} \tag{5}$$

Here, B is the ring thickness while R and R_0 are the inner and outer radii of the ring, respectively.

Following Torabi et al.,[36] Kirsch's solution together with Hobbs' correction [32] are used to determine the tensile stress distribution $\sigma_x(y)$ along the loading axis y (see the schematic of the ring specimen shown in Fig. 1-a for the definition of the axes x and y):

$$\sigma_x(y) = \frac{\sigma_{\max}}{2}\left(2 - 2\frac{R^2}{y^2} + 12\frac{R^4}{y^4}\right)F_{\text{corr}} \tag{6}$$

Here, F_{corr} is a correction factor that should be taken into account for sufficiently large R/R_0 ratios, which follows:

$$F_{\text{corr}} = 1 + \frac{19}{3}\left(\frac{R}{R_0}\right)^2. \tag{7}$$

In the course of the ring experiments, we observe an interesting phenomenon that we would like to discuss. As shown in Figs. 2-b and 2-d, the mechanical response of the ring specimen with the largest inner radius shows two peaks, the first one being larger than the second one. It turns out that full failure of the ring specimen took place in two steps. First, as the load is increased, the tensile strength of the material is reached and failure takes place at point A (see Fig. 2-c). After stress drop, the sample is still able to sustain load. As a result, the applied load increases again, starting from a lower level until it reaches a second time the tensile strength of the material at point C (see Fig. 2-c). It is interesting to notice that each half of the sample can still bear some compressive load until the tensile strength of the material is reached a second time at point C, and providing a good evidence that the sample has been split under pure tension at point A.

The first and second peaks in Fig. 2-d corresponds to the fractures labelled in Fig. 2-c and located at points A and C, respectively. From this observation, it can be concluded that ring test is suitable to measure the tensile strength. From recorded videos by high-speed cameras, we do observe that rings with smaller internal holes are always separating from point A in a tensile mode as well (Fig. 3), as expected from direct numerical simulations of failure in such specimens.[33]

2.3. Semi-circular bending test

The notched semi-circular geometry is used for preparing rock specimens with high-stress concentrators. Various methods have been used to determine the fracture toughness of rock materials.[e.g. 28,37-39] The method

suggested by ISRM [28] relies on SCB specimens that is rather simple to machine and provides good repeatability.[e.g. 40-43]

Herein, SCB specimens are prepared and tested according to ISRM. Multiple SCB specimens for each rock type are tested and the average generalized (or apparent) fracture toughness $K_{\mathrm{Ic}}^{\mathrm{U}}$ is calculated as follows:

$$K_{\mathrm{Ic}}^{\mathrm{U}} = Y' \frac{P_{\max}\sqrt{\pi a}}{DB} \tag{8}$$

Here a, B, D, and $P_{\max}$ are the notch length, the specimen thickness, the diameter of the SCB specimen and the maximum applied load, respectively (see Fig. 4). The notch length of the tested SCB specimens is comprised between 14 to 16 mm while the notch tip radius is 350 microns. The diameter and the thickness of the SCB specimens range from 74 to 76 mm and 29 to 31 mm, respectively. Finally, Y' gives the non-dimensional stress intensity factor derived using the finite element method while assuming plane-strain conditions.[28] Its expression follows:

$$Y' = -1.297 + 9.516(s/D) - \big(0.47 + 16.457(s/D)\big)\beta + \big(1.071 + 34.401(s/D)\big)\beta^2 \tag{9}$$

where s is the span length which is between 37 to 38 mm for all our tests while β is equal to $2a/D$.

Failure of SCB specimens is recorded by means of a high-speed camera (Fig 5-a). It can be clearly seen that the fracture initiates from the notch tip and propagates parallel to the axis of application of the forces, as expected. Typical load-extension curves obtained for different rock types are shown in Fig 5-b.

Creager–Paris solution [24] provides the stress distribution in SCB specimens with a blunted notch of radius ρ:

$$\sigma(x,0) = \frac{2K^{\mathrm{U}}}{\sqrt{\pi}} \frac{x+\rho}{(2x+\rho)^{3/2}} \tag{10}$$

using the coordinate system depicted in Fig. 4-b. K^{U}, the apparent stress intensity factor, is provided by Eq. (8) after replacing the failure load $P_{\max}$ by the current applied load P.

2.4. Direct fracture toughness measurement using SCB tests

To test the ability of the proposed methodology to accurately measure the fracture toughness of rock materials, we proceed to an independent measurement of K_{Ic} using the failure load of the semi-circular bending tests. The basic idea is to consider that at the onset of failure, the imposed stress intensity factor (determined from Eqs. (8) and (9) at the tip of the notch) reaches the fracture toughness value K_{Ic}. However, in our experiments, the notch tip radius is too large to be neglected. Compiling a large set of experimental data, Gomez et al.[25] determined the ratio of the apparent fracture toughness (resulting from the finite notch root radius) over the actual material fracture toughness:

$$\frac{K_{\mathrm{Ic}}^{\mathrm{U}}}{K_{\mathrm{Ic}}} = \sqrt{1 + \frac{\pi}{4}\frac{\rho}{(K_{\mathrm{Ic}}/\sigma_{\mathrm{c}})^2}} \tag{11}$$

Here, the intrinsic tensile strength σ_{c} is determined using the PM based methodology while ρ measured from 2D slices of SCB specimens scanned by means of X-ray tomography, is found to be close to 350 microns (Fig. 4-d). $K_{\mathrm{Ic}}^{\mathrm{U}}$ corresponds to the apparent fracture toughness measured experimentally. As the material fracture toughness K_{Ic} appears on both sides of this equation, Eq. (11) must be solved iteratively following the procedure described in Appendix B and illustrated in Figs. 6-a and 6-b. It turns out that the ratio $K_{\mathrm{Ic}}/K_{\mathrm{Ic}}^{\mathrm{U}}$ is close to 0.95 for the four materials investigated.

Beyond the particular cases of the fracture tests carried in this study, Figs. 6-c and 6-d depicts the effect of the cohesive length in comparison to the notch root radius on the ratio $K_{\mathrm{Ic}}/K_{\mathrm{Ic}}^{\mathrm{U}}$. In particular, it can be seen that small notch radii compared to cohesive length give rise to $K_{\mathrm{Ic}} \approx K_{\mathrm{Ic}}^{\mathrm{U}}$.

3. Results and discussion

3.1. Size effect on tensile strength measurements using ring specimens

A natural first step in assessing the structure-independent tensile strength of the rock materials investigated is to determine the apparent (structure dependent) tensile strength σ_{max} as a function of the ring geometry. Ring specimens with various inner radii as well as disk specimens from different rock types are tested for such a purpose. Fig. 7-a shows the value of σ_{max} as a function of the inner hole radius as obtained after averaging over different samples. It appears that the apparent tensile strength strongly depends on the hole radius (Fig. 7-b). This calls for a more advanced method of analysis to determine the inherent tensile strength.

3.2. Intrinsic tensile strength and material fracture toughness

208 The methodology described in Section 2.1 based on the SCB specimens with a notch root radius of 350
209 microns (high concentrator) and the ring specimens with inner radii of 13–15mm (low concentrator) is applied
210 in Fig. 8 for the four rocks investigated. According to Eq. (1), the intersection point of the tensile stress
211 distributions at the onset of failure for both ring and SCB specimens provides both the inherent tensile strength
212 and the cohesive zone length. The fracture toughness value is then obtained from Eq. (3) using the D–B
213 relationship. The results obtained for the four rocks investigated are summarized in Table 1.

214 The validity of the proposed methodology is now tested. First, we compare the fracture toughness value
215 predicted by Eq. (3) with the fracture toughness value measured directly from the notched SCB specimen, after
216 taking into account the effect of its finite notch root radius. For this purpose, the value of σ_c determined
217 previously is used in Eq. (11), providing the ratio $K_{\mathrm{Ic}}/K_{\mathrm{Ic}}^{\mathrm{U}}$ between the inherent fracture toughness and the
218 apparent one, as explained in Sec. 2.4. The comparison shown in Table 2 is excellent. We then compare in Table
219 3 the cohesive zone length as measured from our method using the intersection point between both stress
220 distributions at the onset of failure (see Fig. 8) with the one predicted from D–B Formula using the fracture
221 toughness determined directly from the notched SCB tests and modified for the rounded notch tip effect. Here
222 also, the agreement is very good. Last but not least, we did proceed to an independent measurement of the
223 process zone length from statistical fractography, a technique that consists in analysing the statistics of fracture
224 surface roughness to extract the characteristic size of the damage processes taking place at the crack tip vicinity
225 during propagation, and found values comparable to the one determined in this study, i.e. in the range 0.7 – 1
226 mm.

227 These results call for a few comments. First, the intrinsic tensile strength varies in the range 8 – 25 MPa
228 for the different rock materials investigated. This is somehow larger, however comparable to the values reported
229 in the literature for such materials.[6, 44] Note that using smaller hole radius for the low stress concentrator gives
230 larger values of σ_c, as inferred from Fig. 9 where the tensile stress distribution at the onset of failure is
231 represented for the different specimen geometries. First, considering stronger stress concentrator is not
232 compatible with the justification of Eq. (1) that requires the combination of a high and a low stress concentrator
233 (see Section 2.1). Second, it leads to smaller values of cohesive length, of the order of a few hundred of microns,
234 that do not match with the results inferred from the statistical analysis of the fracture surfaces.

235 We then would like to discuss the fracture toughness values measured for the four rocks investigated. Our
236 methodology provides accurate fracture toughness values, in agreement with values of K_{Ic} determined directly
237 from the notched SCB specimens using the ISRM suggested method. Afterwards, it turns out that the value of
238 the apparent fracture toughness obtained with a notch root radius less than 500 microns as suggested by ISRM
239 already provides a rather good estimate of K_{Ic} for the rocks investigated. Overall, precision achieved by both
240 methods is remarkable.

241

3.3. Discussion

So far, the results are interpreted and it is concluded that PM is successful in order to measuring intrinsic tensile strength and material fracture toughness, especially when the D–B formula is being used to determine the material fracture toughness. This conclusion can open new doors for future researches and needs further enlightening. The main questions should be answered concerning these results are: 1) Why PM is successful? 2) Why D–B formula is giving better results?

To answer these fundamental questions, first, we need to give a brief background of PM, and both original and developed methods used to calculate the characteristic length L. As discussed in section 2, Eq. (1) introduced by Peterson [45] is the main failure criterion of PM. This formula is considering a material dependent characteristic length inferring the estimated stress for a particular geometry at a distance $L/2$ from its concentrator is equal to inherent tensile strength of the material. In this argument, L is a constant characteristic length depends on intrinsic properties of a material, and is independent from geometry of specimen. Therefore, for homogeneous materials, stress distribution, as a function of distance from concentrator, of any two different geometries would intersect at a point showing material properties. The abscissa of this point is half of the material characteristic length and its ordinate is intrinsic tensile strength.

Although PM is successful in practice, from above presentation, there are two major facts lacking applicability and supportive theoretical arguments. First, materials are not homogeneous and there should be always some rooms for experimental calibrations, even though one uses the highest and lowest possible stress concentrators for determining the intersection point as it is done in this study. Second, how the L should be determined to further estimate material fracture toughness and why $L/2$ is corresponding to material tensile strength. The first issue concerning applicability of this model is out of scope of this study and will be addressed in a future work. From the results of this study, the second issue turns out to be very important and can increase the accuracy of PM with some modifications. Not solid, but it is reasonable to consider the stress at half of the characteristic length L would be equal to intrinsic tensile strength. It is somehow representing the average stress over L that lead to failure of material. It is notable that this argument is close to CZM assumptions for derivation of Eq. 3 (refer to Appendix A).

Barenblatt [9] and Dugdale [31] separately and at the same time have developed basis for the CZM. Their models have different theoretical arguments and physics but treat the problem with similar procedures. Barenblatt model is looking at the problem at microscopic scale and considers inter-molecular cohesive stresses at a large enough area for applying continuum fracture mechanics, and is suitable for brittle materials. Dugdale model is a macroscopic model and considers perfectly plastic material behaviour inside the process zone ahead of crack tip. In these models, the process zone (the cohesive zone in Barenblatt model or the plastic zone in Dugdale model) in direction of applied load (y) is small compared to its length in crack propagation direction (x). Moreover, in Barenblat model the length of cohesive zone is small in comparison to crack length $\ell_c \ll a$,

and the distribution of cohesive stress σ_c in the cohesive zone for a given material is always the same and independent of the external load.[46] These two models in the most simplified scenario (strip or line model) will be end up with the same closed form solution, and this is why Eq. (3) referred to as D–B formula (refer to Appendix A).

Overall, considering CZM and PM descriptions it makes sense to employ D–B formula instead of Eq. (2) for calculating the characteristic length. On the one hand, PM asserts L is material dependent and can be determined by testing specimens from same material but different geometries. On the other hand, Barenblatt model argues distribution of σ_c in the cohesive zone for a given material is always the same and depends on material properties. Finally, although these formulas considering different stress distributions over L or ℓ_c, both Eq. (1) and Eq. (3) are considering average stress at $L/2$ at the moment of failure, and it seems D–B model assumptions are closer to reality.

4 Conclusions

In this study, a TCD based methodology is examined to determine two key mechanical properties of rock materials namely intrinsic tensile strength and material fracture toughness. The first and foremost conclusion is that PM form of TCD is a suitable means to reliably determine intrinsic tensile strength and material fracture toughness of different rock types. According to our results, PM is very reliable if the cohesive length ℓ_c is considered as the characteristic length L in this method.

Following the results of this study, it turns out that plane disk specimens without stress concentrators cannot be used to measure tensile strength of rock materials, and tensile strength is underestimated if plane specimens are used. However, it could provide engineers with a safe and conservative estimation despite the fact that it would often increase the costs of a project. From the observations in the course of ring experiments, it can be concluded that ring test is a suitable means to measure apparent tensile strength of rock materials. Tensile strength of rocks revealed to depend on their structural properties due to the facts discussed by Hudson.[11] However, if a specific value should be reported for a particular rock type and is needed by analytical or numerical solutions, then intrinsic tensile strength of the rock can be determined following the procedure in this study with the aid of newly developed PM.

Brittle nature of rock materials is a major issue for fabricating sharp notch in SCB specimens to successfully determine material fracture toughness. In this study, notch mechanics and practical developments in similar materials were introduced to circumvent this difficulty. From the experimental observations and comparison with different methods, it is being suggested that Gomez et al.[25] formula can be used to successfully rectify the notch root radius effect on determining fracture toughness of rock materials. However, if the notch root radius is smaller than the cohesive length, the ISRM suggested method [28] is a reliable method for determining fracture

toughness of rock materials. Based on the results of this study, the cohesive length is around 1mm for rock materials. Therefore, if the notch width is less than 1mm or notch root radius is less than 500 microns, as specified in the ISRM suggested method,[28] then the material fracture toughness measured by this method is reasonably close to the real value.

Although, the results are satisfying, there is a mismatch between the actual location and the considered intersection point for estimating the intrinsic tensile strength because of material heterogeneities and theoretical assumptions. This is why fracture toughness values estimated from SCB tests modified for notch root effect and developed PM are a bit different. The question remains open in this study is that how this issue can be rectified and if there is any way to measure L or ℓ_c for different materials to get the best possible results. In other words, the length of the fracture process zone in the direction of crack propagation or the cohesive length ℓ_c should be quantified to determine the actual stress at the tip of cohesive zone right before failure of a material in order to precisely measure the material fracture toughness. Further investigations and future researches are required to exactly quantify the length of fracture process zone and answer this question.

Acknowledgements

S. A. wishes to acknowledge the support from Australian Government Research Training Program (RTP) Scholarship and the Monash International Tuition Scholarship (MITS). This research was financially supported by the Australian Research Council (DE200101293), Australian Synchrotron, the MASSIVE HPC facility (www.massive.org.au), and the Monash Centre for Electron Microscopy (MCEM).

Declaration of competing interest

The authors would like to declare that there is no conflict of interests regarding publication of this article.

Appendix A

Following Taylor,[30] derivation of Eq. (2) starts by Westergaard's equation [47] that provides estimation of tensile stress $\sigma(r)$ in the direction of crack propagation as a function of distance r from the crack tip, for a through-thickness crack of a half-length a in an infinite body. The equation can be read as:

$$\sigma(r) = \sigma\sqrt{\frac{a}{2r}} \tag{A1}$$

if $r \ll a$ i.e. for the comparatively close points to the crack tip for an applied tensile stress σ.

According to LEFM for the same conditions mode I stress intensity factor K_{I} can be calculated:

$$K_{\mathrm{I}} = \sigma\sqrt{\pi a} \tag{A2}$$

At the moment of failure K_{I} and σ can be replaced by critical mode one stress intensity factor or fracture toughness K_{Ic} and tensile failure stress σ_f, respectively:

$$K_{\mathrm{Ic}} = \sigma_f\sqrt{\pi a} \tag{A3}$$

Finally, combining the PM criterion Eq. (1) with Eqs. (A1 and A3), σ_f^2 is equal to both side of the Eq. (A4):

$$\frac{L{\sigma_0}^2}{a} = \frac{{K_{Ic}}^2}{\pi a} \tag{A4}$$

which is another form of the Eq. (2).

Derivation of Eq. (3) can be summarized as follows. If a crack or notch with length a as shown in Fig. A1 is considered, then distribution of $\sigma_{\mathrm{c}}(x, 0)$ along ℓ_{c} ranged from the physical crack tip or notch tip to fictitious crack tip would be non-linear. The general formula for calculating mode I stress-intensity factor associated with such cohesive stresses $K_{\mathrm{I}}^{\mathrm{c}}$ for a straight crack in an infinite body can be formulated as follows:[1]

$$K_{\mathrm{I}}^{\mathrm{c}} = -2\sqrt{(c/\pi)}\int_0^c \frac{\sigma_{\mathrm{c}}(x,0)}{\sqrt{c^2 - x^2}}dx \tag{A5}$$

where $c = a + \ell_{\mathrm{c}}$ and $\sqrt{c^2 - x^2}$ is Green's function. There is no close form solution for this equation since the distribution of σ_c over ℓ_{c} is unknown. The D–B formula is derived by simplifying this condition. If we consider σ_{c} over ℓ_{c} has a constant value (strip model), then Eq. (A5) will transform to:

$$K_{\mathrm{I}}^{\mathrm{c}} = -\sqrt{(2/\pi)}\int_{a}^{c}\frac{\sigma_{\mathrm{c}}(x,0)}{\sqrt{x}}dx \tag{A6}$$

Fig. A2 shows this simplified situation for a crack of length $2(a+\ell_{\mathrm{c}}) = 2c$ in an infinite body under uniaxial tensile stress σ. Then, using superposition of the problem, and right before crack propagation, the following equilibrium could be reached:

$$K_{\mathrm{I}} = -K_{\mathrm{I}}^{\mathrm{c}} \tag{A7}$$

where K_{I} is given in Eq. (A2) and $K_{\mathrm{I}}^{\mathrm{c}}$ can be solved using Eq. A6. Now, the equilibrium can be rewritten as follows:

$$\sigma\sqrt{\pi c} = 2\sigma_{\mathrm{c}}\sqrt{\frac{c}{\pi}}\cos^{-1}\frac{a}{c}; \tag{A8}$$

$$\rightarrow \sqrt{\pi c}\left(\sigma - \frac{2\sigma_{\mathrm{c}}}{\pi}\cos^{-1}\frac{a}{c}\right) = 0;$$

$$\therefore \frac{a}{a+\ell_{\mathrm{c}}} = \cos\left(\frac{\pi\sigma}{2\sigma_{\mathrm{c}}}\right)$$

Finally, by two reasonable assumptions including $\ell_{\mathrm{c}} \ll a$ and $\sigma \ll \sigma_{\mathrm{c}}$ this equilibrium can be solved for ℓ_{c}:

$$1 - \frac{\ell_{\mathrm{c}}}{a} = 1 - \frac{\pi^2\sigma^2}{8\sigma_{\mathrm{c}}^2}; \tag{A9}$$

$$\rightarrow \ell_{\mathrm{c}} = \frac{\pi\sigma^2\pi a}{8\sigma_{\mathrm{c}}^2}$$

that is another form of Eq. (3).

Appendix B

The iterative method for estimating material fracture toughness K_{Ic} from Gomez et al.[25] practical formula (Eq. 11) can be presented as follows. First of all, Eq. 11 can be divided in the two following formulas:

$$\frac{K_{Ic}^{U}}{K_{Ic}} = \sqrt{1 + \frac{\pi}{4}\frac{\rho}{l_{\mathrm{ch}}}} \tag{B1}$$

where l_{ch} is a characteristic length given in Eq. B2:

$$l_{\mathrm{ch}} = (K_{\mathrm{Ic}}/\sigma_{\mathrm{c}})^2. \tag{B2}$$

Then, an iterative process for estimating K_{Ic} can be presented in four steps as follows:

a) estimating the l_{ch} using Eq. (B2) by assuming K_{Ic} is equal to the measured generalized fracture toughness from experiment;
b) estimating the material fracture toughness by replacing the measured generalized fracture toughness from experiment, notch tip radius ρ, and the calculated l_{ch} from the first step into Eq. (B1);
c) updating the l_{ch} by replacing the estimated material fracture toughness from the second step into Eq. (B2); and
d) repeating this loop several times until old and new l_{ch} values and accordingly material fracture toughness values converge.

The larger the ρ or the smaller the l_{ch}, the greater the number of required iterations for convergence (see Fig. 4-a).

This method has a limitation that is connected to the ratio of ρ/l_{ch}. Based on some numerical examples, it turns out that this iterative process works well if ρ is smaller or slightly larger than l_{ch}. It is notable that if $\rho = l_{\mathrm{ch}}$, then $K_{\mathrm{Ic}}/K_{\mathrm{c}}^{\mathrm{U}} \approx 0.5$ (after convergence).

References

1. Lawn B. Fracture of Brittle Solids. London: Cambridge University Press; 1993.

2. Myer LR, Kemeny JM, Zheng Z, Suarez R, Ewy RT, Cook NGW. Extensile cracking in porous rock under differential compressive stress. Appl Mech Rev 1992;45(8):263–280.

381 3. Haimson BC, Cornet FH. ISRM suggested methods for rock stress estimation—Part 3: hydraulic fracturing
382 (HF) and/or hydraulic testing of pre-existing fractures (HTPF). Int J Rock Mech Min Sci. 2003;40:1011–
383 1020.

384 4. Weibull W. A statistical distribution function of wide applicability. J Appl Mech. 1951;18(3):293–297.

385 5. Bazant ZP, Planas J. Fracture and Size Effect in Concrete and Other Quasibrittle Materials. Boca Raton
386 Florida: CRC Press; 1997.

387 6. Perras M, Diederichs M. A review of the tensile strength of rock: concepts and testing. Geotech Geol Eng.
388 2014;32:525–546.

389 7. Justo J, Castro J, Cicero S. Application of the Theory of Critical Distances for the Fracture Assessment of a
390 Notched Limestone Subjected to Different Temperatures and Mixed Mode with Predominant Mode I
391 Loading Conditions. Rock Mech Rock Eng. 2021; https://doi.org/10.1007/s00603-021-02365-7.

392 8. Atkinson BK. Subcritical crack growth in geological materials. J Geophys Res: Solid Earth.
393 1984;89(B6):4077–4114.

394 9. Barenblatt GI. The mathematical theory of equilibrium cracks in brittle fracture. Adv Appl Mech. 1962;7:55–
395 129.

396 10. Xu XP, Needleman A. Numerical simulations of fast crack growth in brittle solids. J Mech Phys Solids.
397 1994;42(9):1397–1434.

398 11. Hudson JA. Tensile strength and the ring test. Int J Rock Mech Min Sci Geomech Abstr. 1969;6:91–97.

399 12. Taylor D. The theory of critical distances. Eng Fract Mech. 2008;75:1696–1705.

400 13. Ibáñez-Gutiérrez FT, Cicero S, Carrascal IA, Procopio I. Effect of fibre content and notch radius in the
401 fracture behaviour of short glass fibre reinforced polyamide 6: an approach from the Theory of Critical
402 Distances. Comp Part B: Eng. 2016; 94:299–311.

403 14. Ibáñez-Gutiérrez FT, Cicero S, Carrascal IA. On the influence of moisture content on the fracture behaviour
404 of notched short glass fibre reinforced polyamide 6. Comp Part B: Eng. 2019;159:62–71.

405 15. Susmel L, Taylor D. Fatigue design in the presence of stress concentrations. Int J Strain Analy. 2003;38:443–
406 452.

407 16. Susmel L, Taylor D. On the use of the theory of critical distances to predict static failures in ductile
408 metallic materials containing different geometrical features. Eng Fract Mech. 2008;75:4410–4421.

409 17. Pereira JCR, de Jesus AMP, Xavier J, Correia JAFO, Susmel L, Fernandes AA. Low and ultra-low-cycle
410 fatigue behavior of X52 piping steel based on theory of critical distances. Int J Fatigue. 2020;134:1–9.

411 18. Cicero S, Torabi AR, Madrazo V, Azizi P. Prediction of fracture loads in PMMA Unotched specimens using
412 the equivalent material concept and the theory of critical distances combined criterion. Fatigue Fract Eng
413 Mater Struct. 2017;1–12.

414 19. Peron M, Torgersen J, Berto F. A novel approach for assessing the fatigue behavior of PEEK in a
415 physiologically relevant environment. Materials. 2018;11:1923.

416 20. Cicero S, García T, Castro J, Madrazo V, Andrés D. Analysis of notch effect on the fracture behaviour of
417 granite and limestone: an approach from the theory of critical distances. Eng Geol. 2014;177:1–9.

418 21. Jenkins A, Fathi E, Belyadi F. Stress field behavior induced by hydraulic fracture in shale reservoirs: a
419 practical view on cluster spacing. J Nat Gas Sci Eng. 2017;48:186–196.

420 22. Justo J, Castro J, Cicero S, Sánchez-Carro MA, Husillos R. Notch effect on the fracture of several rocks:
421 application of the theory of critical distances. Theor Appl Fract Mech. 2017;90:251–258.

422 23. Justo J, Castro J, Cicero S. Notch effect and fracture load predictions of rock beams at different temperatures
423 using the theory of critical distances. Int J Rock Mech Min Sci. 2020;125:104161.

424 24. Creager M, Paris P. Elastic field equations for blunt cracks with reference to stress corrosion cracking. Int J
425 Fract Mech. 1967;3:247–252.

426 25. Gomez FJ, Guinea GV, Elices M. Failure criteria for linear elastic materials with Unotches. Int J Fract.
427 2006;141:99–113.

428 26. Lazzarin P, Filippi S. A generalized stress intensity factor to be applied to roundedV-shaped notches. Int J
429 Solids Struct. 2006;43:2461–2478.

430 27. Tanné E, Li T, Bourdin B, Marigo JJ, Maurini C. Crack nucleation in variational phase-field models of
431 brittle fracture. J Mech Phys Solids. 2018;110:80–99.

432 28. Kuruppu MD, Obara Y, Ayatollahi MR, Chong KP, Funatsu T. ISRM-suggested method for determining
433 the Mode I static fracture toughness using semi-circular bend specimen. Rock Mech Rock Eng.
434 2014;47(1):267–274.

435 29. Taylor D. Predicting the fracture strength of ceramic materials using the theory of critical distances. Eng
436 Fract Mech. 2004;71:2407–2416.

30. Taylor D. The Theory of Critical Distances: A New Perspective in Fracture Mechanics. Oxford, UK: Elsevier; 2007.

31. Dugdale DS. Yielding of steel sheets containing slits. J Mech Phys Solids. 1960;8:100–104.

32. Hobbs DW. An assessment of a technique for determining the tensile strength of rock. Br J Appl Phys. 1965;16:259–268.

33. Zhang XJ, Yi YN, Zhu HB, Liu GY, Sun LB, Shi L, Jiang H, Ma SP. Measurement of tensile strength of nuclear graphite based on ring compression test. J Nucl Mater. 2018;511:134–140.

34. Bai QS, Tu SH, Zhang C. DEM investigation of the fracture mechanism of rock disc containing hole(s) and its influence on tensile strength. Theor Appl Fract Mec. 2016;86:197–216.

35. Filon LNG. The stresses in a circular ring. Sel Engng Pap Instn Civ Engrs. 1924;Paper No. 12.

36. Torabi AR, Etesam S, Sapora A, Cornetti P. Size effects on brittle fracture of Brazilian disk samples containing a circular hole. Eng Fract Mech. 2017;496–503.

37. ISRM. The complete ISRM suggested methods for rock characterization, testing and monitoring: 1974–2006. In: R. Ulusay, J.A. Hudson (eds) Suggested methods prepared by the commission on testing methods, International Society for Rock Mechanics, compilation arranged by the ISRM Turkish National Group. Kozan Ofset, Ankara: 2007.

38. Nara Y, Kaneko K. Study of subcritical crack growth in andesite using the Double Torsion test. Int J Rock Mech Min Sci. 2005;42:521-530.

39. Ponson L. Depinning transition in the failure of inhomogeneous brittle materials. Phys Rev Lett. 2009;103:055501.

40. Chong KP, Kuruppu MD, New specimen for fracture toughness determination for rock and other materials. Int J Fract. 1984; 26(2):R59–R62.

41. Aliha MRM, Hosseinpour GR, Ayatollahi MR. Application of cracked triangular specimen subjected to three-point bending for investigating fracture behavior of rock materials. Rock Mech Rock Eng. 2013;46(5):1023–1034.

42. Zhang QB, Zhao J. Effect of loading rate on fracture toughness and failure micromechanisms in marble. Eng Fract Mech. 2013;102:288–309.

464 43. Nejati M, Aminzadeh A, Driesner T, Saar MO. On the directional dependency of Mode I fracture toughness
465 in anisotropic rocks. Theor Appl Fract Mech. 2020;107:102494.

466 44. Li D, Wong LNY. The Brazilian disc test for rock Mechanics applications: review and new insights. Rock
467 Mech Rock Eng. 2013;46(2):269–287.

468 45. Peterson RE. Notch-sensitivity. In Metal Fatigue (Edited by Sines G and Waisman JL.). New York: McGraw
469 Hill; 1959;293–306.

470 46. Gross D, Seelig T. Fracture Mechanics With an Introduction to Micromechanics, Third ed. Berlin: Springer-
471 Verlag; 2018.

472 47. Westergaard HM. Bearing Pressures and Cracks, J Appl Mech. 1939;6:49–53.

List of Figures

List of Tables

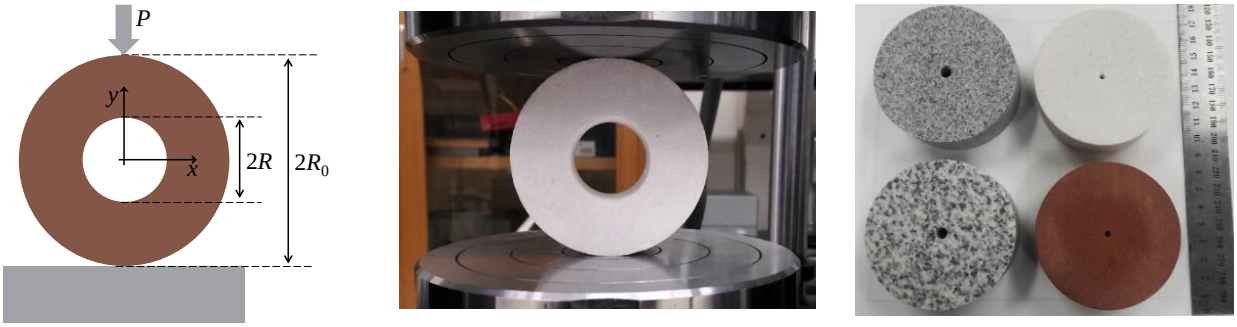

(a) (b) (c)

511 Fig. 1. Ring experiment: (a) Schematic of the ring specimen; (b) A marble ring with an inner radius of 15mm
512 under compression; and (c) Specimens with the minimum inner radii before testing.

513

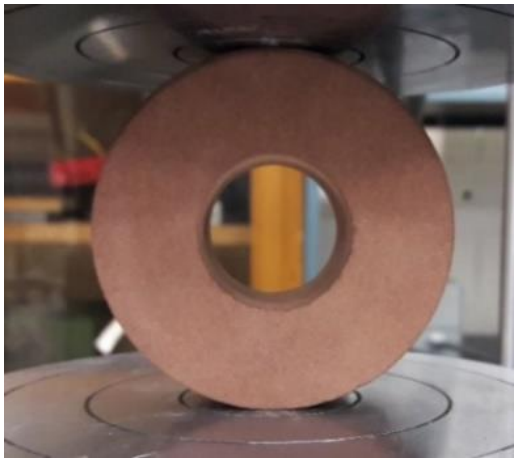

(a)

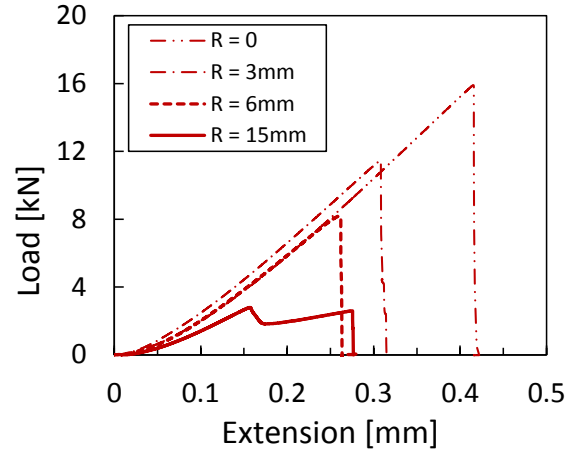

(b)

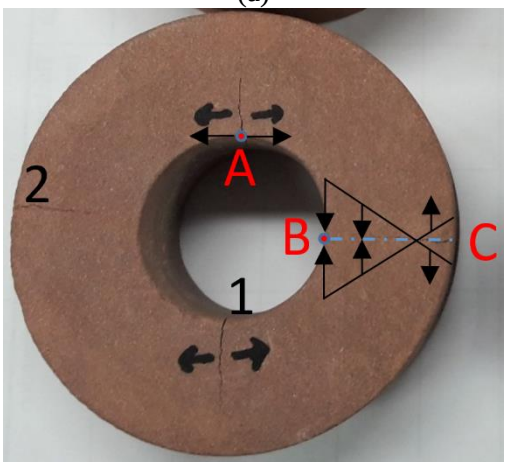

(c)

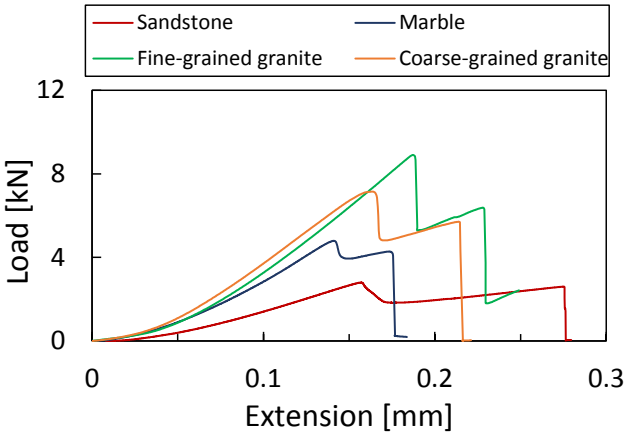

(d)

514 Fig. 2. a) Sandstone ring specimen under compression; b) Mechanical response of the sandstone ring specimens
515 with different inner radii; c) Schematic illustration of the two steps failure behaviour of ring specimens; and d)
516 Mechanical response of the ring specimens made of different rocks for the largest inner radii (13-15mm).

517

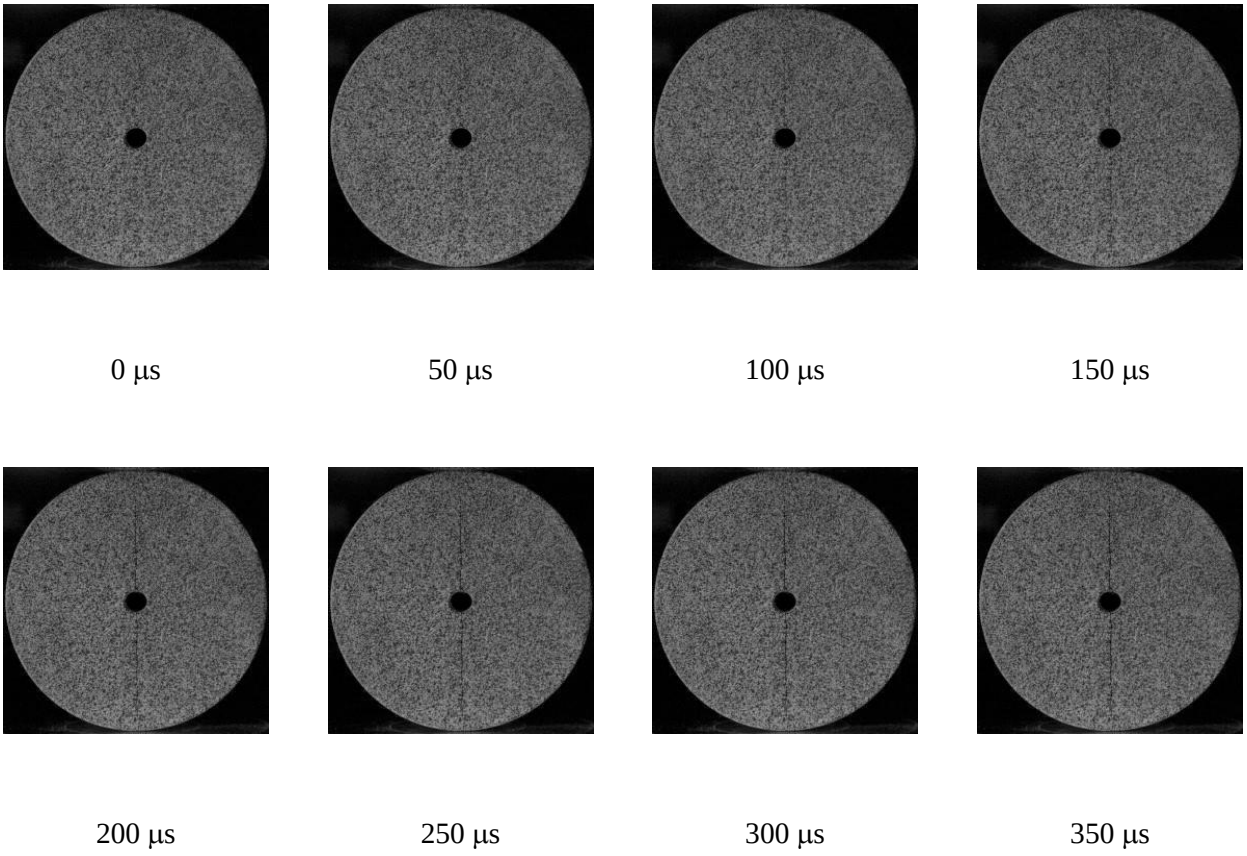

Fig. 3. Sequence of high-speed images taken from a sandstone ring with an inner radius of 3 mm showing symmetric fracture propagation from point A, as depicted in Fig. 2-c.

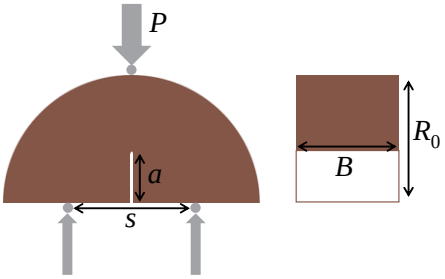

(a)

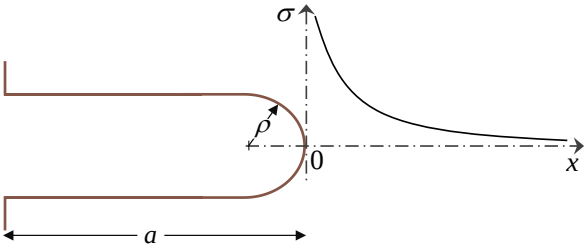

(b)

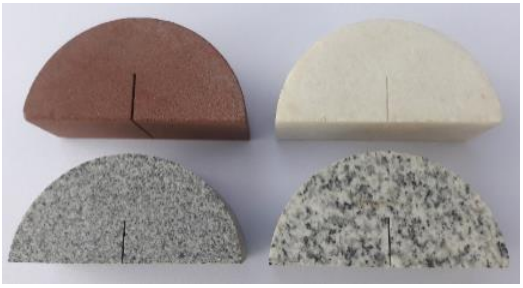

(c)

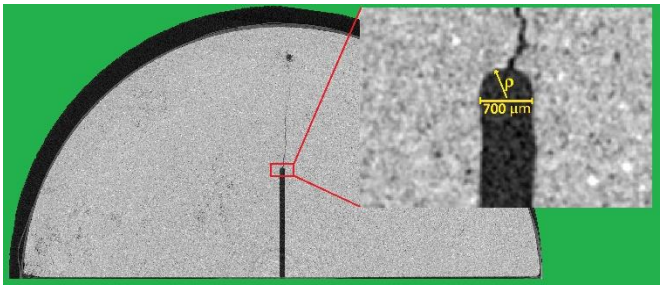

(d)

522 Fig. 4. SCB fracture tests: (a) Schematic of SCB specimen under three point bending; (b) Schematic of the stress
523 distribution on the bisector line of a blunted notch under opening mode loading conditions; (c) SCB specimens
524 before testing; and (d) 2D image slice of a sandstone SCB specimen scanned by means of X-ray tomography
525 after failure. Note the radius $\rho \approx 350\mu m$ of the initial notch.

526

527

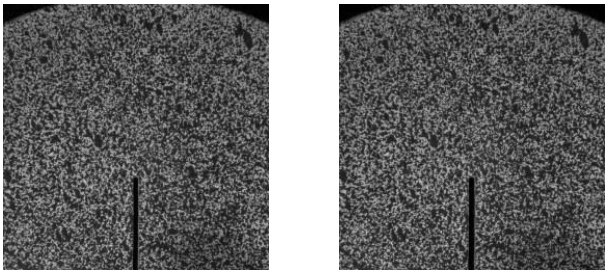

0 μs 200 μs

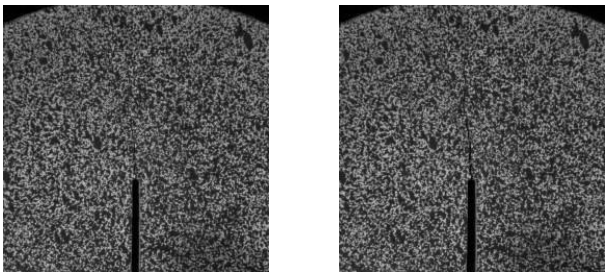

400 μs 600 μs

(a)

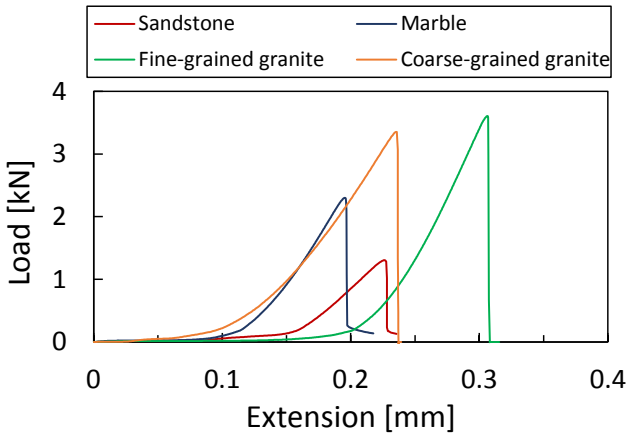

(b)

528 Fig. 5. (a) Sequence of high-speed images taken from a fine-grained granite SCB specimen showing crack
529 initiation and growth from the initial notch tip; (b) Mechanical response of the notched SCB specimens for the
530 four rocks investigated.

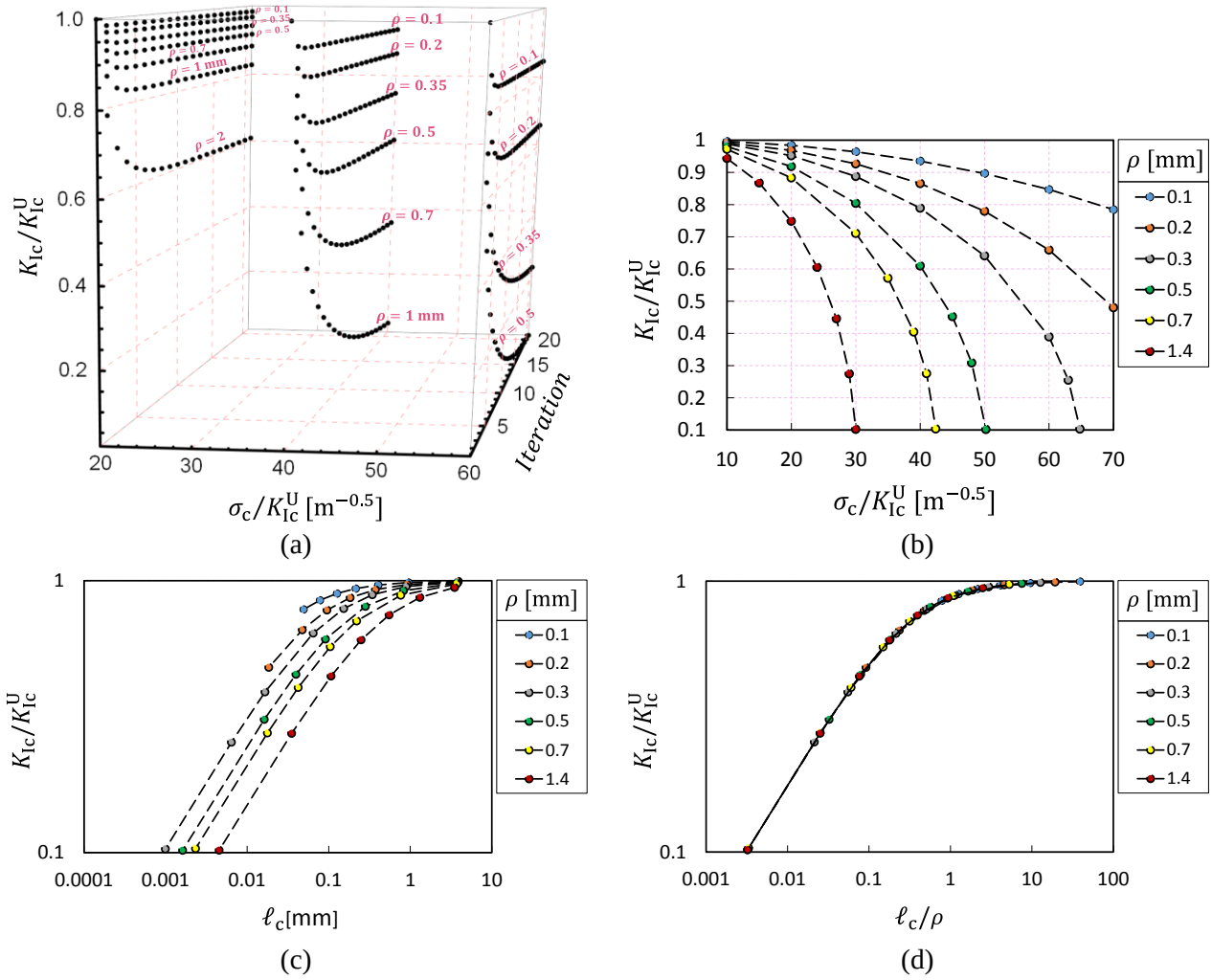

Fig. 6. Graphical guides for modifying the notch root radius effect on material fracture toughness: a) A 3D guide showing the iterative process; and b) A guide for estimating K_{Ic} as a function of notch tip radius, intrinsic tensile strength and generalized fracture toughness. c) K_{Ic} as a function of notch tip radius, the cohesive length and generalized fracture toughness; and d) A single master curve for evaluating K_{Ic} as a function of ℓ_c/ρ ratio and generalized fracture toughness.

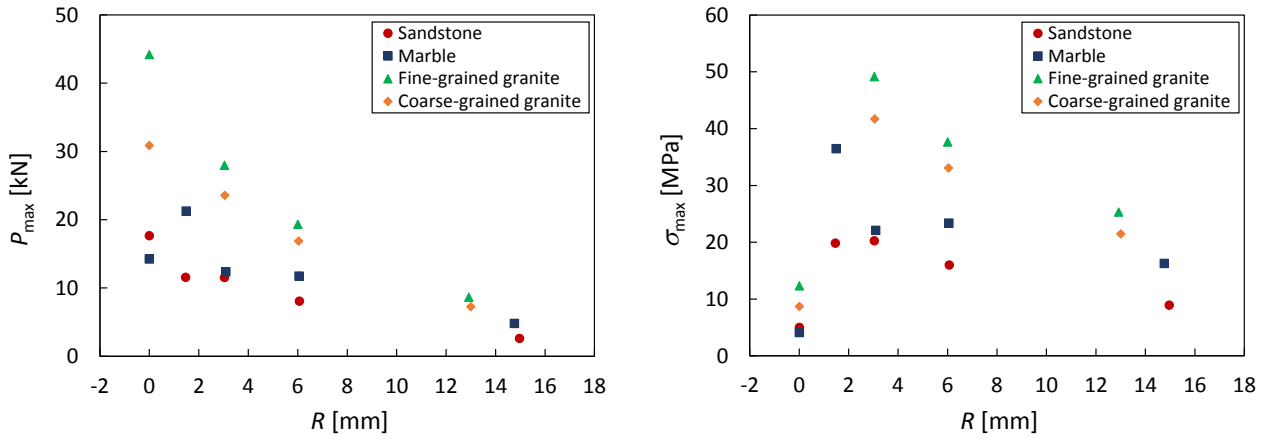

537 Fig. 7. Failure load P_{max} (a) and apparent tensile strength σ_{max} (b) of the different rocks investigated as obtained
538 from the different fracture tests.

539

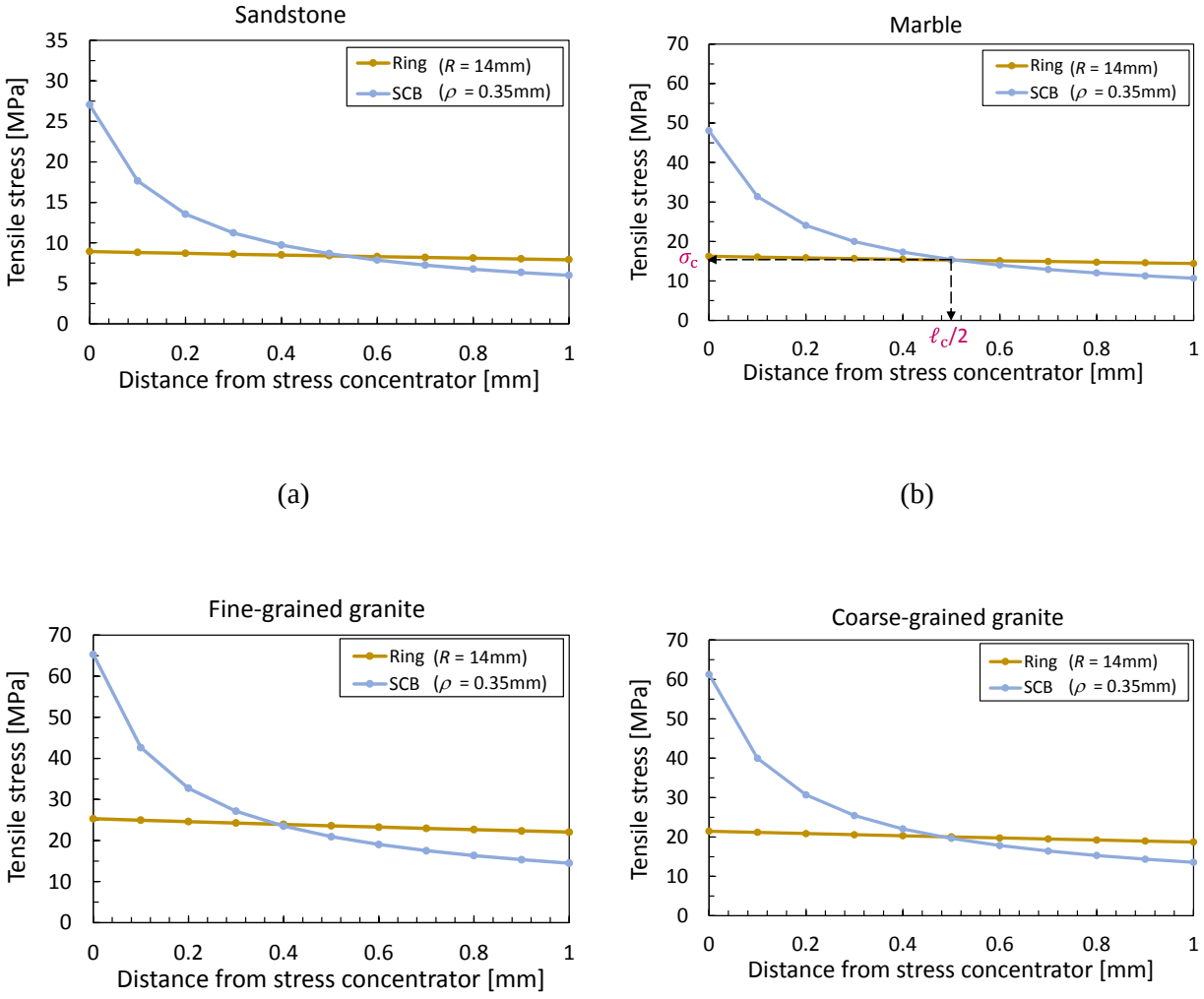

Fig. 8. Application of the PM for the determination of the tensile strength: Stress distribution against distance for the two geometries displaying the highest and the lowest stress concentrations for (a) sandstone, (b) marble, (c) fine-grained granite and (d) coarse-grained granite. The point of intersection of both curves provide the intrinsic tensile strength as well as the cohesive length, as illustrated for marble in the panel (b).

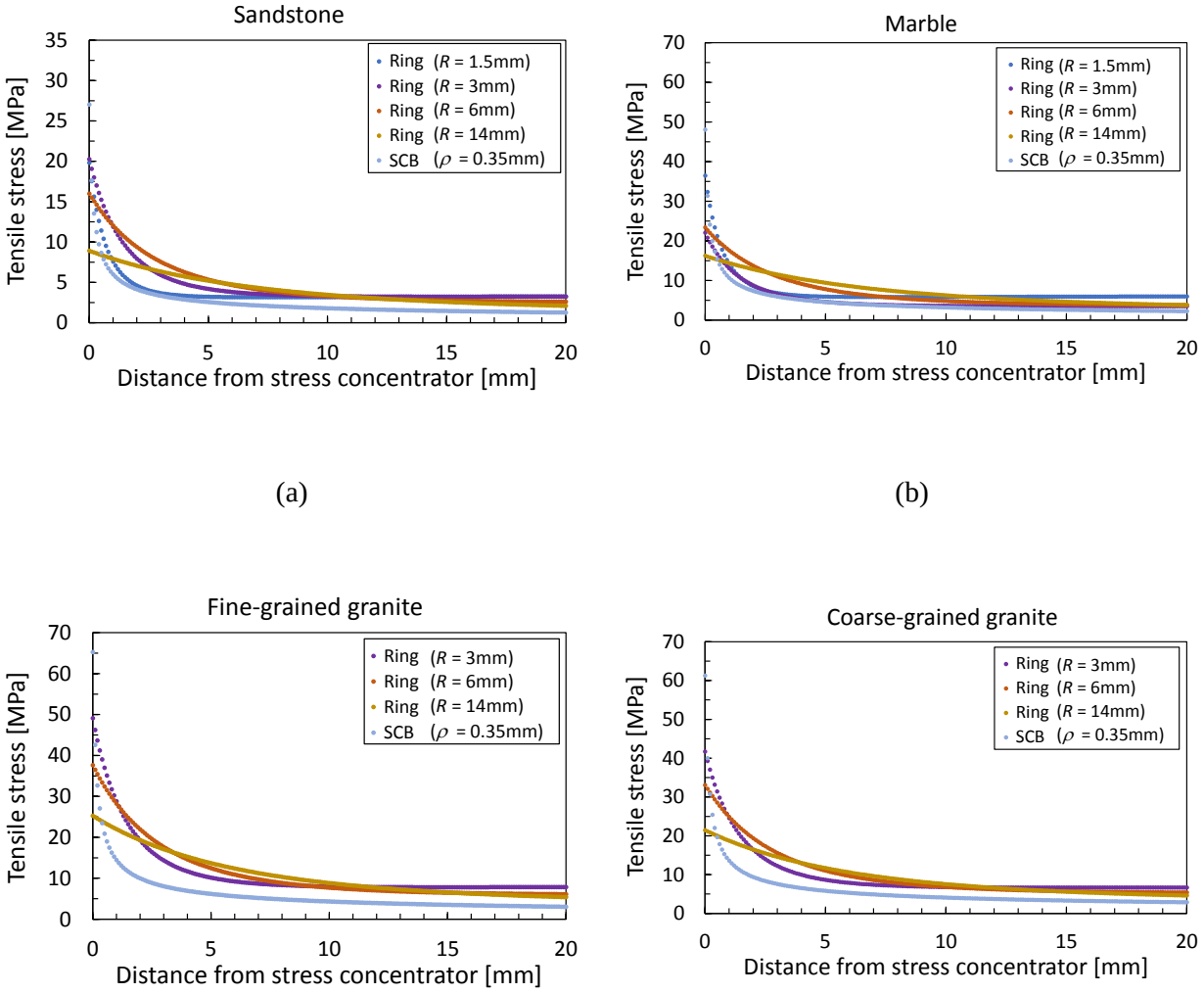

545 Fig. 9. Tensile Stress distribution against distance at the onset of failure for different fracture test geometries
546 and different materials: a) sandstone; b) marble; c) fine-grained granite; and d) coarse-grained granite.

547

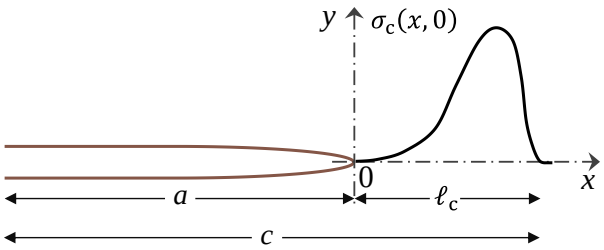

Fig. A1. Schematic of Barenblat cohesive zone model.

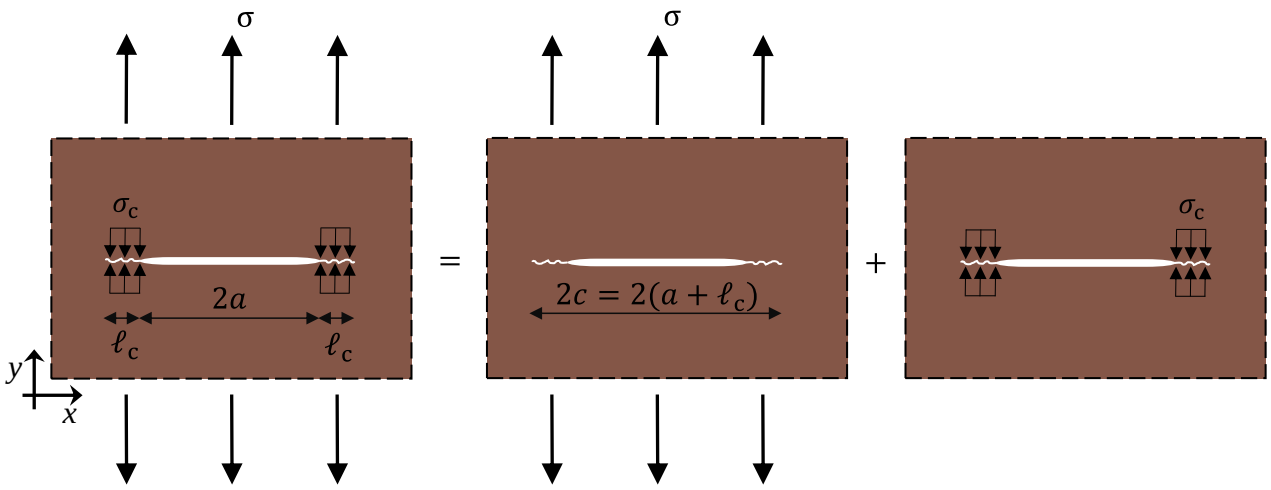

551

552 Fig. A2. Equilibrium for derivation of D–B formula as superposition of applied tensile and cohesive stresses.

553

554 Table 1. The intrinsic tensile strength, the cohesive half-length and the material fracture toughness, determined
555 by the developed PM.

Rock type	σ_c [MPa]	$\ell_c/2$ [mm]	K_{Ic} [MPa.m$^{0.5}$]
Sandstone	8.4	0.53	0.44
Marble	15.4	0.51	0.78
Fine grained granite	24.0	0.39	1.07
Coarse grained granite	19.8	0.48	0.98

556

557

Table 2. Comparison of measured generalized fracture toughness K_{Ic}^{U} [MPa.m$^{0.5}$] and modified fracture toughness K_{Ic} [MPa.m$^{0.5}$] values with those obtained using the common and developed PMs.

Rock type	K_{Ic}^{U} (ISRM [28])	K_{Ic} (Gomez et al.[25])	K_{Ic} (common PM)	K_{Ic} (developed PM)
Sandstone	0.45	0.43	0.49	0.44
Marble	0.80	0.76	0.86	0.78
Fine grained granite	1.08	1.00	1.19	1.07
Coarse grained granite	1.02	0.97	1.11	0.98

561 Table 3. The cohesive length ℓ_c [mm] as per D–B formula determined both from SCB tests modified for the
562 rounded notch tip effect and the developed PM.

Rock type	Experimental	Developed PM
Sandstone	1.03	1.07
Marble	0.96	1.01
Fine grained granite	0.68	0.78
Coarse grained granite	0.94	0.96

563

Graphical Abstract PDF

Performing experiments

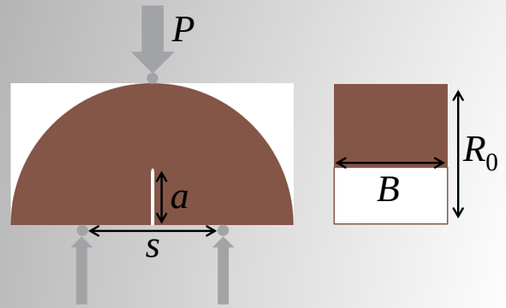

SCB test: High stress concentration

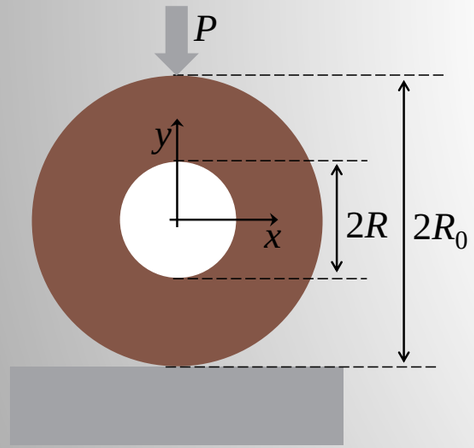

Ring test: Low stress concentration

Applying Point Method

Stress distribution vs. distance from concentrator

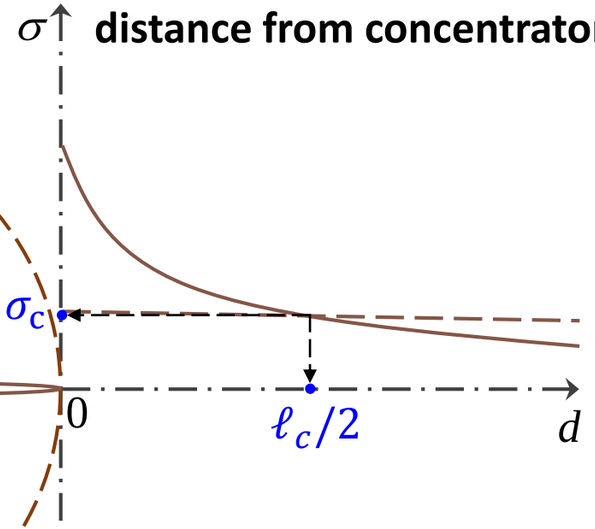

SCB test:

$$\sigma(d,0)=\frac{2K_{Ic}^{U}}{\sqrt{\pi}}\frac{d+\rho}{(2d+\rho)^{3/2}}$$

Creager–Paris solution

Ring test:

$$\sigma(d,0)=\frac{\sigma_{max}}{2}\left(2-2\frac{R^2}{d^2}+12\frac{R^4}{d^4}\right)\left(1+\frac{19}{3}\left(\frac{R}{R_0}\right)^2\right)$$

Kirsch's solution and Hobbs' correction

Modifying PM

$$\sigma(\ell_c/2)=\sigma_c$$

Estimating fracture toughness

$$K_{Ic}=f(\ell_c,\sigma_c)$$

Validating the results

K_{Ic}(Experimental) ≈ K_{Ic}(Developed PM)